43rd IEEE Conference on Decision and Control
December 14-17, 2004
Atlantis, Paradise Island, Bahamas

Steady-State Multiplicity and Stability of Thermal Equilibria in Homogeneous Charge Compression Ignition (HCCI) Engines

C. J. Chiang and A. G. Stefanopoulou
University of Michigan, Ann Arbor
Email: cjchiang,annastef@umich.edu

Abstract— **The stability of the autothermic process governing the autoignition of HCCI engines is analyzed in this paper. We find conditions under which steady-state multiplicity exists with stable, unstable, and limit-cycle equilibria. This analysis is conducted taking into account the internal feedback structure of the thermal autoignition dynamics. Specifically, HCCI autoignition timing determines the combustion heat produced and is determined by the heat provided through high internal exhaust gas recirculation from previous combustion cycle.**

It is shown that the thermal equilibria are characterized by a simple returning map consisting of two curves, namely the breathing temperature curve and the combustion temperature curve. The returning map and the stability analysis of the multiple steady state equilibria is confirmed with a high order dynamic nonlinear model that includes manifold filling and composition dynamics.

I. Introduction

The 'flameless' spontaneous combustion of HCCI engines is based on autoignition where the combustion initiation depends on kinetically driven oxidation process [1]. The reactivity depends on the heat absorbed and it is not followed by violent energy release typically characterized as knock [2]. The autoignition principle does not rely on flame propagation [3] thus allows combustion in a homogeneous mixture similar to Spark Ignition (SI) engines. On the other hand, due to the autoignition nature, HCCI engines sustain high compression ratio similar to Compression Ignition (CI) engines, and thus obtain high thermal efficiency. In other words, HCCI engine is a hybrid of the SI and CI engine concept [4]. In fact, the HCCI engine integrates the advantages of both the CI and the SI engine [5]: (i) High fuel efficiency by using high compression ratio and rapid heat release [4]. (ii) Low NOx and low particulate matter (PM) emissions due to low cylinder peak temperature [4]. (iii) Fuel flexible and may be cost competitive to manufacturing since a high pressure fuel injection system is not required as in a CI engine [6].

The main difficulty in controlling the HCCI combustion is that ignition cannot be actuated directly. The autoignition timing of HCCI combustion is determined by the cylinder charge conditions, rather than the spark timing or the fuel injection timing that are used to initiate combustion in SI and CI engines, respectively [7]. Instead, controlled autoignition requires regulation of the charge properties, namely, temperature, pressure, and composition at the Intake Valve Closing (IVC) as demonstrated by many experimental results [5], [2].

Thring [5] found that HCCI is highly dependent on exhaust gas recirculation (EGR) rate and intake air temperature. Najt *et al.* in [2] explored the effects of several parameters on the ignition process and energy release of a HCCI engine and concluded that charge temperature is the primary mechanism for controlling ignition timing. Charge temperature can be controlled by high dilution and thus recirculation of hot exhaust gas [8], [7]. One such method is a secondary opening of the exhaust valve during the intake stroke (rebreathing). Using high dilution levels the exhaust gas heat can increase the charge temperature for the next cycle, and thus determine the ignition and the exhaust temperature of the subsequent cycle [9].

The HCCI engines can, thus, be viewed as stirred chemical reactors [2] and considered as Thermal Ignition (TI) engines. Their start-up and asymptotic characteristics can be analyzed with simple returning maps reported in the early 20^{th} century by Liljenroth [10] and used more recently by Kantor in [11] for a potential explanation of the origin of cycle-to-cycle variability in SI engines. Thermal autoignition equilibria and their stability can be described by a returning map that captures the temperature effect of the prior combustion to the next via the exhaust gas recirculation.

In the combustion and automotive literature there are many citations about the stability of the HCCI combustion and especially the dynamic connection between subsequent combustion cycles during transients. For example, in [12] the authors stress the importance of taking into account the combustion of the previous cycle. Due to the large amount of residuals (or internal exhaust gas recirculation) a combustion event depends largely on the chemical and thermal state of the prior combustion cycle. Although there is a strong evidence that partially oxidized fuel from misfiring cycles can affect the ignition of the charge in the next cycle [13] leading to limit cycles, we neglect the coupling through the chemical energy in this paper. We, instead, concentrate on the cycle-to-cycle coupling introduced by the thermal energy of the residuals.

Assuming fast manifold dynamics and accurate air-to-fuel ratio control we show that HCCI temperature dynamics can be analyzed by the return map consisting of two curves, namely the breathing temperature curve and the combustion temperature curve. The first curve provides the cylinder charge temperature at intake valve closing (T_{ivc}) as it is governed by the breathing characteristics of the engine. The

0-7803-8682-5/04/$20.00 ©2004 IEEE

second curve provides the charge temperature in the exhaust runner (T_{er}) as it is governed by the combustion following the auto-ignition of the compressed charge. The block diagram in Fig. 1 shows the two interacting temperature variables in the internal feedback constituted by the residual gas trapped in the cylinder as developed by Rausen *et al.* in [9]. This internal feedback exists in a small percentage in conventional SI or CI engines, but its effects are pronounced in HCCI due to the large percentage of residual gas in the cylinder charge[1].

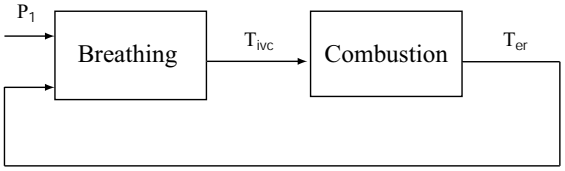

Fig. 1. The thermal feedback introduced by the breathing characteristics and the combustion characteristics of the HCCI engine with large percentage of residual gas in the cylinder charge.

The gain of the $\frac{\partial T_{er}}{\partial T_{ivc}} \frac{\partial T_{ivc}}{\partial T_{er}}$ defines the stability of the open loop HCCI dynamics. Specifically, $|\frac{\partial T_{er}}{\partial T_{ivc}} \frac{\partial T_{ivc}}{\partial T_{er}}| < 1$ causes a passive system associated with negative feedback and thus contributes to the stability of the system. We follow the work on stability of autothermal chemical reactors [14], [15], [16], and use the mean value model (MVM) [9], which relies on the average values of cylinder flows in each cycle, to find the thermal equilibria of the HCCI engine.

Our results corroborate many combustion stability results in the combustion literature based on experiment data. For example, Willand *et al.* [1] claimed that "Late combustion provides hot exhaust gas causing the next cycle to ignite earlier and reduce exhaust gas temperature again." In other words, the timing of start of combustion (SOC) controlled internally through the retained exhaust gas, also known as internal EGR (iEGR), is self-stabilizing and thus more robust. Also, Thring [5] explored the operating limits of an HCCI engine by varying EGR and AFR. He observed that "...deep in the knock zone, knock could become excessively heavy, and engine combustion timing would become more and more advanced until the engine would finally stop firing altogether." More recently, Olsson *et al.* [4] discovered by experiments that "The energy exchange or storage can drive the combustion event to instability...While in some cases operation is stable and very easy to control, other operating conditions require fast and accurate feedback control to maintain steady state operation."

Although many experiments have been performed to design HCCI engines and develop steady-state operating maps, no stability analysis has been done to support or explain the experimentally observed dynamic behavior of autoignition based HCCI engine. Our paper fills this gap by offering analytical basis for understanding the HCCI engine dynamics.

[1]Up to 60% dilution is achieved during the rebreathing valve event in HCCI engines.

II. Approach and Nomenclature

The model we use to analyze the open loop stability of an HCCI engine is the MVM model constructed by Rausen *et al.* [9] where the cylinder is modeled based on cycle-average cylinder flows as shown in Fig. 2. Flows from volume x to volume y are denoted as W_{xy}. There are three relevant volumes: (i) the intake manifold denoted with subscript 1, (ii) the exhaust manifold denoted with subscript 2, (iii) the cylinder denoted with subscript c. The atmospheric conditions are denoted with subscript 0. Each flow is calculated by the effective flow area and standard orifice equation. The fuel flow rate is denoted as W_f.

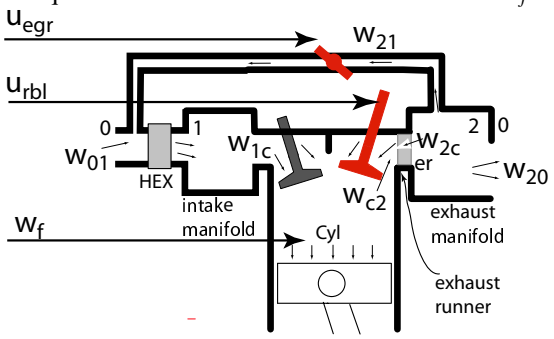

Fig. 2. Schematic representation of the engine.

High percentage of residual mass is trapped in the cylinder by a secondary opening of the exhaust valve during the intake stroke. The lift of the secondary opening is called rebreathing lift (RBL). The control signal associated with the actuator for the rebreathing lift is denoted as u_{rbl} in Fig. 2. A conventional exhaust gas recirculation (EGR) valve based on the control signal u_{egr} (shown in Fig. 2) affects the burned gas fraction in the intake manifold. The EGR flow mixes with the fresh air and passes through a heat exchanger (HEX) that controls the inlet manifold temperature at 90^o C. Thus, the rebreathing lift (RBL) allows control of the internal EGR (iEGR– hot dilution from one cycle to the next cycle) and the conventional exhaust gas recirculation valve (EGR) allows control of the external EGR (eEGR–dilution at 90^o C through the exhaust and intake manifolds).

The pressure dynamics associated with the intake and exhaust manifold filling process are, in general, much faster than the temperature dynamics. We, thus, assume that the intake and exhaust manifold pressure and mass filling dynamics converge at their steady state equilibtium points within a cycle. Therefore, only the charge temperature at intake valve closing T_{ivc} and exhaust runner temperature T_{er} are the two dominant, cycle-to-cycle dynamics. The MVM model was developed based on experimental data from an engine with insulated exhaust manifold and exhaust runners. The absence of exhaust manifold cooling implies that the temperature of the solid wall material in the cylinder and runner follows the exhaust gas temperature. The gas constant R and heat capacity are assumed to be constant. We also assume fixed intake valve closing timing θ_{ivc}.

To analyze the autonomous system dynamics, operating conditions such as fueling rate, intake manifold pressure, and actuator setting are chosen within the range of existing experimental data [9]. For this study the intake manifold pressure P_1 ranges from 100.1 to 100.8 kPa due to unthrottled conditions, and atmosphere pressure, P_0 is kept at 101.0 kPa.

III. Breathing Characteristics

Here we construct the breathing block of the system in Fig. 1, which maps T_{er} to T_{ivc}. Since the intake manifold temperature, T_1, is assumed to be constant at 90°C through a heat exchanger, the charge temperature in the cylinder at intake valve closing, T_{ivc} is determined solely by the residual mass trapped, m_{res} and the exhaust temperature, T_{er}:

$$T_{ivc} = \frac{T_1 m_{im} + T_{er} m_{res}}{m_{im} + m_{res}} \ , \tag{1}$$

where the cylinder mass m_{im} associated with the flow from the intake manifold to the cylinders (W_{1c}) during a period of cycle τ is given by

$$m_{im} = W_{1c}\tau \ . \tag{2}$$

The mass of gas from the rebreathing flow m_{res}, also called residual mass, is calculated based on the ideal gas law and Dalton's law of the partial pressures of the gas from the intake manifold P_{im}, and the gas from the rebreathing flow P_{res} as they contribute to the total in-cylinder pressure at IVC (P_{ivc}):

$$\begin{aligned} m_{res} &= \frac{P_{res}V_{ivc}}{RT_{er}} = \frac{(P_{ivc} - P_{im})V_{ivc}}{RT_{er}} \\ &= \frac{P_{ivc}V_{ivc}}{RT_{er}} - m_{im}\frac{T_1}{T_{er}} = \frac{P_{ivc}V_{ivc}}{RT_{er}} - W_{1c}\tau\frac{T_1}{T_{er}} \ . \end{aligned} \tag{3}$$

The in-cylinder pressure at IVC, P_{ivc}, is approximated well as a linear function of the intake manifold pressure P_1 using experimental data [9]:

$$P_{ivc} = \beta_0 + \beta_1 P_1 \ . \tag{4}$$

By substituting (2) and (3) to (1) we obtain the expression for the temperature in the cylinder at intake valve closing, T_{ivc} as

$$T_{ivc} = \frac{(\beta_0 + \beta_1 P_1)V_{ivc}T_{er}}{W_{1c}\tau R(T_{er} - T_1) + (\beta_0 + \beta_1 P_1)V_{ivc}} \ . \tag{5}$$

The mass flow from the intake manifold to the cylinder, W_{1c} can be expressed as a function of P_1 and T_{er} by solving the following steady-state flow equations. First, the continuity of mass at the intake manifold gives us

$$W_{1c} = W_{01}(P_0, T_0, P_1) + W_{21}(P_2, T_2, P_1) \ , \tag{6}$$

where P_2 is related to P_1 and T_2 by the continuity of total mass in and out of the engine:

$$W_{20}(P_2, T_2, P_0) = W_{01}(P_0, T_0, P_1) + W_f \ . \tag{7}$$

Note that W_{01}, W_{21}, and W_{20} are calculated using the orifice equation ([17], Appendix C) for constant effective flow coefficients. Finally, the exhaust manifold temperature T_2 is

$$T_2 = T_{er} - \Delta T_{er2} \tag{8}$$

where $\Delta T_{er2} = 75^\circ$ C is a temperature drop from the exhaust runner temperature (T_{er}) to the exhaust manifold temperature (T_2) observed in the steady-state experimental data.

Equation (5)-(8) define the breathing characteristics that describe T_{ivc} based on T_{er} and P_1. Fig. 3 shows the breathing map between T_{ivc} and T_{er} for fixed fuel flow rate at 9.1 mg/cycle. Note that the curve moves upward when P_1 increases. For comparison, the case when external EGR is set to zero ($u_{EGR} = 0$) is also plotted. Note here that although external EGR is set to zero, high percentage of residual gas is still trapped in the cylinder due to the rebreathing event.

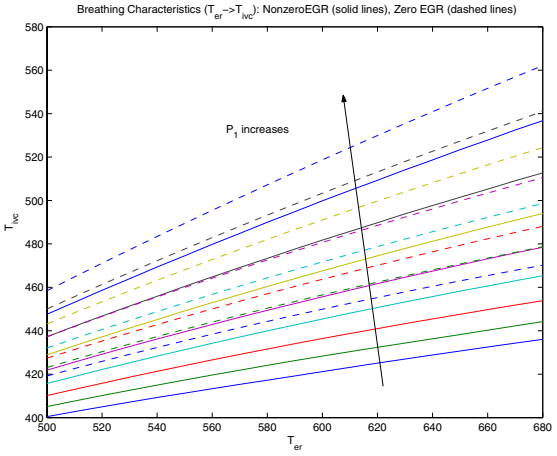

Fig. 3. Breathing Characteristics: $T_{ivc} = f_b(T_{er})$ for fuel flow rate fixed at 9.1 mg/cycle. The case when EGR=13 mm^2 is plotted in solid line and when EGR=0 mm^2 is plotted in dashed line. Note here that, although EGR is set to zero, high percentage of residual gas is still trapped in the cylinder due to the rebreathing event.

IV. Combustion Characteristics

To construct the combustion block of the system in Fig. 1 which maps T_{ivc} to T_{er}, a simple phenomenological zero-dimensional model of the HCCI combustion is used [9]. This model, which algebraically maps the conditions at intake valve closing (IVC) to those at exhaust valve opening (EVO), consists of five sequential phases: (i) a polytropic compression that leads to start of combustion (SOC) through autoignition at θ_{soc}, (ii) a combustion duration, (iii) an instantaneous heat release, (iv) a polytropic expansion, and (v) an adiabatic blowdown that yields T_{er}. These phases are depicted in Fig. 4, where the actual experimental (solid line) and modeled (dotted line) pressure and temperature trajectories are shown.

Phase 1, Intake Valve Closing to Start of Combustion: Assuming fixed intake valve closing timing θ_{ivc}, the start of combustion θ_{soc} of the homogeneous charge is related to the pressure and temperature at IVC with the integral [18]:

$$\int_{\theta_{ivc}}^{\theta_{soc}} A P_{ivc}^{n} v_{ivc}^{n_c n}(\vartheta) exp(-\frac{E_a v_{ivc}^{1-n_c}(\vartheta)}{R_a T_{ivc}}) d\vartheta = 1 \tag{9}$$

where $E_a = 6317$ J/kg is the activation energy for the autoignition reaction, $n = 1.367$ indicates the reaction's

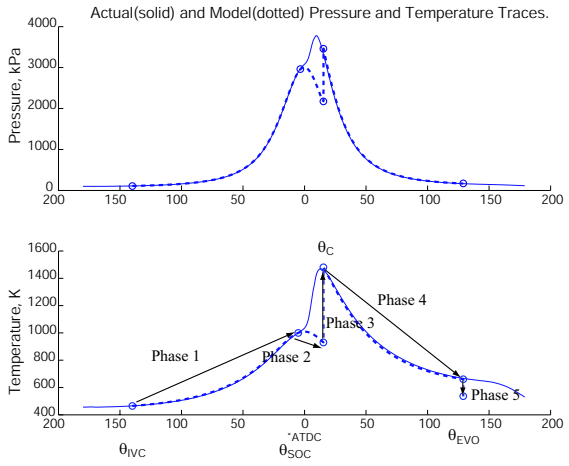

Fig. 4. Actual (solid) and estimated (dotted) pressure and temperature traces in cylinder, from before IVC to after EVO. Calculated (model) values are indicated with circles.

sensitivity to pressure, $A = 2500$ is the Arrhenius scaling constant, $R_a = 296.25$ J/kg-K is the gas constant. We assume a polytropic compression process from IVC to SOC with coefficient $n_c = 1.3$ applied in the cylinder volume ratio $v_{ivc}(\vartheta) = V_c(\vartheta_{ivc})/V_c(\vartheta)$ with $V_c(\vartheta)$ being the cylinder volume at crankangle ϑ. The charge temperature at SOC is then calculated as $T_{soc} = T_{ivc} v_{ivc}^{(n_c-1)}(\theta_{soc})$.

Phase 2 and 3, Combustion Duration and Heat Release: The combustion timing $\theta_c = \theta_{soc} + \Delta\theta$ occurs $\Delta\theta$ degrees after the start of combustion θ_{soc}. Based on experimental data of the crankangle associated with 90% fuel burned, the combustion duration $\Delta\theta$ is calculated using Ronney's model [19], $\Delta\theta = k(T_{soc})^{(-2/3)}(T_m)^{1/3} exp(E_c/(3R_cT_m))$ to capture the almost instantaneous combustion of an HCCI engine, where $E_c = 185$ kJ/mol is the activation energy for combustion reaction, $R_c = 8.314$ J/mol-K is the universal gas constant, and the parameter $k = b_0 + b_1\theta_{soc} + b_2\theta_{soc}^2$ was characterized using experimental data. Following [19], the effective mean temperature is $T_m = T_{soc} + e\Delta T$. The parameter $e = a_0 + a_1 k$ is tuned to capture the apparent fuel efficiency that lumps (i) combustion efficiency and (ii) heat losses through the walls. The coefficients a_0, a_1 and b_0, b_1, b_2 are determined from experiment data in [9]. After the combustion duration, instantaneous heat release occurs with associated temperature increase $\Delta T = Q_{LHV} W_f \tau/(c_v m_c)$, where $m_c = p_{ivc}V_{ivc}/(RT_{ivc})$ is the total trapped mass in cylinder. The charge temperature and pressure just before the combustion are $T_{bc} = T_{ivc} v_{ivc}^{(n_c-1)}(\theta_c)$ and $P_{bc} = P_{ivc} v_{ivc}^{n_c}(\theta_c)$, respectively.

Phase 4, and 5, Heat Release to Exhaust Blowdown: The charge temperature and pressure after the combustion are $T_{ac} = T_{bc} + \Delta T$ and $P_{ac} = P_{bc}T_{ac}/T_{bc}$. Assuming polytropic expansion, the charge temperature and pressure at EVO become $T_{evo} = T_{ac} v_c^{(n_e-1)}(\theta_{evo})$ and $P_{evo} = P_{ac} v_c^{n_e}(\theta_{evo})$ where $v_y(\vartheta_x) = V_c(\vartheta_y)/V_c(\vartheta_x)$. After the exhaust valve opens, the exhaust gas temperature can be modeled through a blowdown process from the cylinder into the exhaust runner and an offset $T_{er} = T_{evo}(P_2/P_{evo})^{(n_e-1)/n_e} - 65$.

These five phases combined with (6)-(8) map T_{ivc} to T_{er} and the mapping is shown in Fig. 5 for fuel flow rate fixed at 9.1 and 11.1 mg/cycle. The curve moves downward when P_1 increases or when fuel flow rate decreases. Note that the combustion curve is invariant to EGR because EGR affects only the T_{ivc} from (5). The non-monotonic shape of the combustion curve can be explained through simple energy conservation arguments. Indeed, if the start of combustion is not timed right more fuel turns to wasted heat and increases the gas temperature in the exhaust runner T_{er}. It is obvious from Fig. 5 that there is a fuel-optimum T_{ivc}^* for which most of the chemical energy of the fuel is converted to useful mechanical work and not exhaust gas heat. It is also anticipated that the magnitude of the slope $|\frac{\partial T_{er}}{\partial T_{ivc}}|$ to the right of T_{ivc}^* (very advanced SOC) will be smaller than the one to the left of T_{ivc}^* (less advanced). This difference in slopes could be more pronounced depending on the heat dissipated through the walls during early combustion.

This non-monotonic behavior is similar to the curve that relates the exhaust port exit gas temperature to spark timing in SI engines (see for example, Fig. 17 in [20]). The implications of the non-monotonic behavior are, however, far more serious for the autothermic HCCI engine, rather than for the externally initiated combustion in SI engine. We see in the following that the multiple intersection between the combustion curve and the breathing curve allows one or two steady-state equilibria with different stability properties.

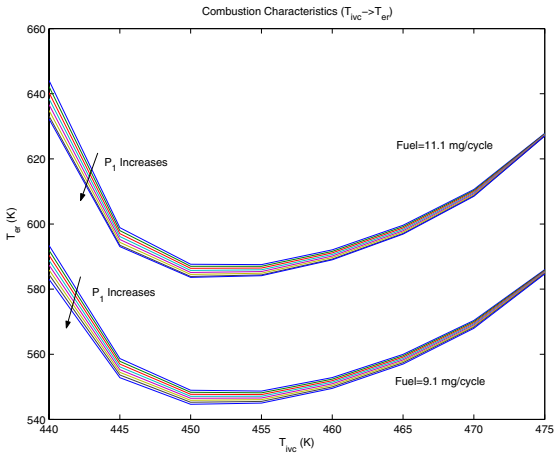

Fig. 5. Combustion Characteristics: $T_{er} = f_c(T_{ivc})$ for fuel flow rate fixed at 9.1 and 11.1 mg/cycle. The curve moves downward when P_1 increases or when fuel flow rate decreases.

V. Steady-State Equilibrium Analysis

Combining the results of the breathing characteristics (solid lines in Fig. 3 with axes being switched) and combustion characteristics (Fig. 5), a graphical representation of the HCCI engine temperature equilibria is obtained, as shown in Fig. 6. The first curve provides the cylinder charge temperature at IVC of cycle k, $T_{ivc}(k) = f_b(T_{er}(k))$ as it is governed by the breathing characteristics of the engine. The second curve provides the charge temperature in the

exhaust runner of the next cycle $T_{er}(k+1) = f_c(T_{ivc}(k))$ as it is governed by the combustion following the auto-ignition of the compressed charge. The intersection of the breathing curve (straight line) and the combustion curve ("U" shape) defines a temperature equilibrium point. As we can see from Fig. 6, for fuel flow rate fixed at 9.1 mg/cycle, the intersection exists when P_1 ranges from 100.4 kPa to 100.7 kPa. This steady-state mapping is verified experimentally only within the area shaded in Fig. 6 ($460^\circ K < T_{ivc} < 470^\circ K$ for fuel flow rate from 9.1 to 11.1 mg/sec). For experimental validation of the model used here see [9]. All the experimental data correspond to stable equilibrium points. More experiment data are currently sought to verify the region outside the grey area.

The stability of an equilibrium point for the recursive mapping is determined by the slopes of the two curves near the intersection. We conclude that stable equilibria exist when $|\frac{\partial T_{er}}{\partial T_{ivc}} \frac{\partial T_{ivc}}{\partial T_{er}}| < 1$. Basically, the equilibrium is stable around the lowest point on the combustion curve (T_{er} at 550°K; T_{ivc} at 450°K). For instance, when P_1 is equal to 100.6 kPa, the intersection of the two curves is a stable equilibrium point, by the temperature converging sequence after a small perturbation from the equilibrium point, as point S_1 in Fig. 7. Unstable equilibrium points appear when P_1 is higher or when the two curves intersect at some point in the right portion of Fig. 6. For example, when P_1 is equal to 100.7 kPa, two intersections of the curves exist and one of them is an unstable equilibrium point from the temperature sequence after a perturbation as point U in Fig. 7. Note that an unstable equilibrium cannot be observed in practice because the noise or environmental variations would cause the trajectory to diverge from the unstable equilibrium even if it is possible to set up the exact initial conditions corresponding to this point [21]. Finally, the recursive mapping indicates oscillatory dynamics or limit cycles when P_1 is lower than 100.5 kPa or when the two curves intersect at some point in the left part of Fig. 6. For example, when P_1 is equal to 100.4 kPa, a limit cycle occurs due to the nonlinearity in the combustion characteristics as shown in Fig. 8. This behavior indicates cycle-to-cycle switching between advanced and retarded autoignition similar to [1]. The predicted magnitude of the temperature oscillation, however, is too large to be observed in reality. Such high temperatures are followed with high heat transfer rates that our model does not include currently. Although the model predicts a limit cycle, other nonlinear phenomena can prevent the limit cycle from happening.

VI. Dynamic Response

To generate the simple two dimensional returning maps above we neglect the intake and exhaust manifold filling dynamics and assume that the equilibrium flow is achieved much faster than the equilibrium temperature. To verify the assumption of instantaneous manifold filling dynamics, we use the full order model to explore if (i) the identified equilibria exist, and if (ii) the full HCCI engine model exhibits stable, unstable, and limit cycle behavior at different equilibria.

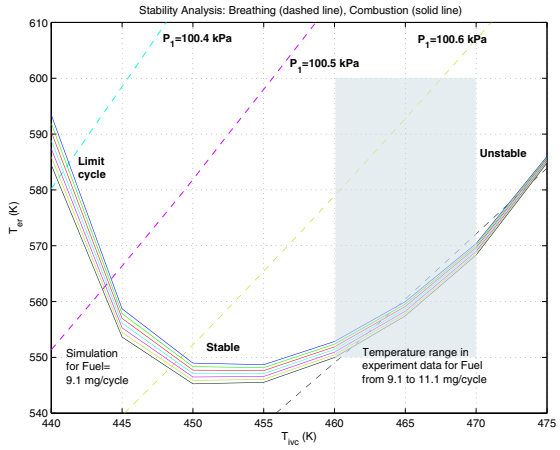

Fig. 6. Stability analysis through the recursive mapping between T_{ivc} and T_{er} for fuel flow rate fixed at 9.1 mg/cycle. This steady-state mapping is verified by experiment only within the shaded area ($460^\circ K < T_{ivc} < 470^\circ K$ for fuel flow rate from 9.1 to 11.1 mg/cycle). More experiment data are currently sought to verify the global behavior outside the grey area.

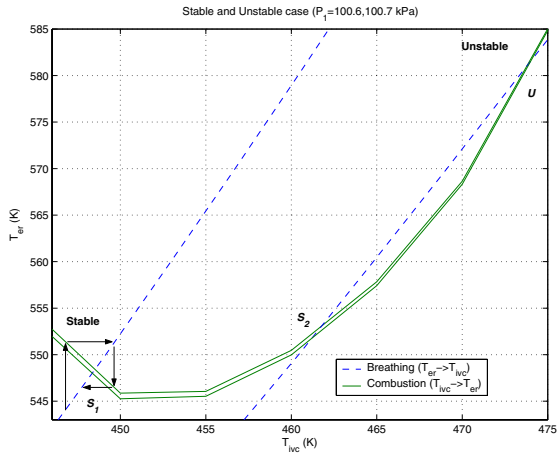

Fig. 7. Stable and Unstable cases (Fuel=9.1 mg/cycle): P_1 equal to 100.6 and 100.7 kPa respectively.

For the same fueling rate and effective flow area we first compute values for the rebreathing lift (RBL) actuator necessary to operate at T_{ivc} and T_{er} that correspond to the stable, unstable and limit cycle equilibria. We then fix the RBL, EGR and fuel inputs to the full order model simulation and initialize T_{er} to the respective operating condition we found in Sec. V.

The simulation results of the full order model match the stability analysis results reported in previous sections except the undamped limit cycle behavior as shown in Fig. 9. Specifically, stable behavior is found for medium combustion temperatures (close to the optimum T^*_{ivc}) and unstable behavior was found for high operating temperature conditions. However, a lightly-damped oscillation was found for low operating temperatures similar to the ones that a limit cycle was predicted before. The damping might be induced by the extra manifold filling dynamics, or we

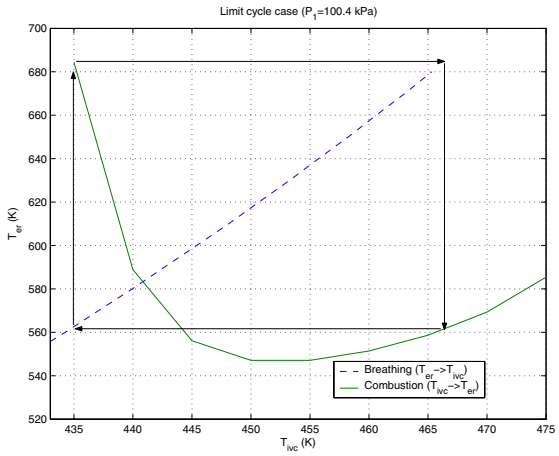

Fig. 8. Limit cycle case (Fuel=9.1 mg/cycle): P_1 equal to 100.4 kPa.

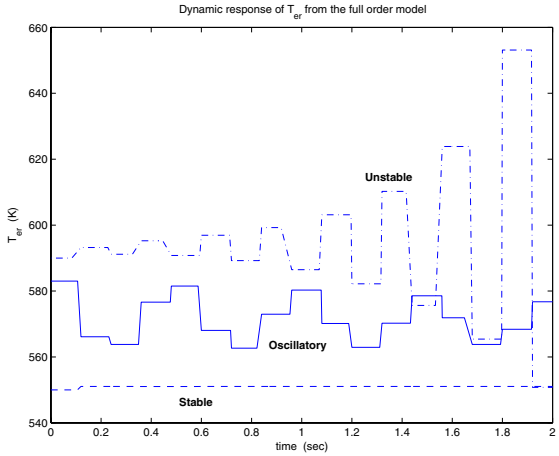

Fig. 9. Simulation response of T_{er} from the full order model for fuel flow rate fixed at 9.1 mg/cycle (RBL equal to 2.33 mm for the stable response, 5.95 mm for the unstable response, and 1.7 mm for the oscillatory response.)

might not have found the exact initial condition for this nonlinear system to operate at limit cycle. More analysis on the region of attraction for the limit cycle is necessary to clarify this issue.

VII. Conclusion

The existence of multiple steady state temperature equilibria and their stability is very important for controller design. For instance, this information clarifies how sensitive the HCCI engine is and how easy it is to move from a stable equilibrium to an unstable equilibrium region due to perturbations coming from model uncertainty and input disturbances. For example, although point S_2 in Fig. 7 is a stable equilibrium, the trajectory can possibly jump to the right side and become unstable due to a fuel increase which causes subsequent increase in T_{er}. In this paper, we assume an insulated exhaust manifold and runner, that allow the cylinder and runner wall temperature to follow the gas temperature. Note here that cooling or high heat transfer rates can change the slope of the breathing loop and combustion loop and affect the system stability.

Our analysis is essential for understanding the HCCI engine operation and crucial for controller design. With better understanding on the region of attraction of the multiple equilibrium points, a robust controller for the HCCI engine can be developed.

Acknowledgment

This work is funded by the General Motors Corporation under contract TCS-09026.

References

[1] J. Willand, R.-G. Nieberding, G. Vent, and C. Enderle, "The knocking syndrome - its cure and its potential," *SAE paper 982483*.

[2] P. Najt and D. Foster, "Compression-ignited homegeneous charge combustion," *SAE paper 830264*.

[3] J. Chen and W. Stevens, "Autoignition and control of flameless combustion," Department of Energy, Tech. Rep., August 2002.

[4] J. O. Olsson, P. Tunestal, B. Johansson, S. Fiveland, R. Agama, M. Willi, and D. Assanis, "Compression ratio influence on maximum load of a natural gas fueled HCCI engine," *SAE paper 2002-01-0111*.

[5] R. H. Thring, "Homegeneous-charge compression-ignition (HCCI) engines," *SAE paper 892068*.

[6] M. Y. Au, J. W. Girard, R. Dibble, S. V. Aceves, J. Martinez-Frias, R. Smith, C. Seibel, and U. Maas, "1.9-liter four-cylinder engine operation with exhaust gas recirculation," *SAE paper 2001-01-1894*.

[7] D. S. Stanglmaier and E. Roberts, "Homogenous charge compression ignition (HCCI): Benefits, compromises, and future engine applications," *SAE paper 1999-01-3682*.

[8] J. Martinez-Frias, S. M. Aceves, D. Flowers, J. R. Smith, and R. Dibble, "HCCI control by thermal management," *SAE paper 2000-01-2869*.

[9] D. J. Rausen, A. G. Stefanopoulou, J.-M. Kang, J. A. Eng, and T.-W. Kuo, "A mean-value model for control of homogeneous charge compression ignition (HCCI) engines," in *Proc. of the American Control Conf.*, 2004, pp. 125–131.

[10] F. G. Liljenroth, "Starting and stability phenomena of ammonia-oxidation and similar reactions," *Chemical and Metallurgical Enigineering*, vol. 19, no. 6, pp. 287–293, September 1918.

[11] J. C. Kantor, "A dynamical instability of spark-ignited engines," *Science*, vol. 224, pp. 1233–1235, June 1984.

[12] M. Kaneko, K. Morikawa, J. Itoh, and Y. Saishu, "Study on homogenous charge compression ignition gasoline engine," in *Proceedings of 5th International Symposium on Diagnostics and Modeling of Combustion in Internal Combustion Engines*, Nagoya, Japan, July 2001.

[13] J. Hiltner, R. Agama, F. Mauss, B. Johansson, and M. Christensen, "HCCI operation with natural gas: Fuel composition implications," in *ASME: International Combustion Engine Technology Conference*, Peoria, Illinois, USA, September 2000, pp. 24–27.

[14] C. V. Heerden, "Autothermic processes - properties and reactor design," *Industrial and Engineering Chemistry*, vol. 45, no. 6, pp. 1242–1247, June 1953.

[15] A. Caton and W. H. Ray, "On the dynamic behavior of continuous stirred tank reactors," *Chemical Enigineering Science*, vol. 29, pp. 967–985, 1974.

[16] R. A. Schimitz, "Multiplicity, stability, and sensitivity of states in chemical reacting systems - a review," *Advances in Chemistry*, vol. 148, pp. 156–211, 1976.

[17] J. B. Heywood, *Internal Combustion Engine Fundamentals*. McGraw-Hill Inc, 1988.

[18] J. C. Livengood and P. C. Wu, "Correlation of autoignition phenomena in internal combustion engines and rapid compression machines," in *Proceedings of Fifth International Symposium on Combustion*, 1955, pp. 347–356.

[19] C. Ji and P. D. Ronney, "Modeling of engine cyclic variations by a thermodynamic model," *SAE paper 2002-01-2736*.

[20] J. A. Caton and J. B. Heywood, "Models for heat transfer, mixing and hydrocarbon oxidation in a exhaust port of a spark-ignited engine," *SAE paper 800290*.

[21] H. K. Khalil, *Nonlinear Systems*. Prentice-Hall Inc, 1996.